HHS Public Access

Author manuscript

J Am Chem Soc. Author manuscript; available in PMC 2018 July 26.

Published in final edited form as:

J Am Chem Soc. 2017 July 26; 139(29): 9972–9978. doi:10.1021/jacs.7b04263.

A Mitochondria-Targeted Cryptocyanine-Based Photothermogenic Photosensitizer

Hyo Sung Jung[†,§], **Jae-Hong Lee**[‡], **Kyutae Kim**[‡], **Seyoung Koo**[†], **Peter Verwilst**[†], **Jonathan L. Sessler**[*,§], **Chulhun Kang**[*,‡], and **Jong Seung Kim**[*,†]

[†]Department of Chemistry, Korea University, Seoul 02841, Korea

[‡]The Graduate School of East-West Medical Science, Kyung Hee University, Yongin 17104, Korea

[§]Department of Chemistry, The University of Texas at Austin, Austin, Texas 78712-1224, United States

Abstract

Cryptocyanine-based probes exhibit highly efficient photothermal conversion and represent a new class of photothermal agents for use in photothermal therapy (PTT). With the thermal susceptibility of mitochondria in mind, we have prepared a mitochondria-targeted, NIR-absorbing cryptocyanine probe (**Mito-CCy**) and evaluated its photophysical properties, photothermal conversion efficiency, biological compatibility, cytotoxicity, and mitochondrial localization in HeLa cells. Upon subjecting 0.5 mL of a PBS buffer solution (10 mM, pH 7.4, containing 50% DMSO) of **Mito-CCy** (0.5 mM) to 730 nm laser irradiation at 2.3 W/cm^2, the temperature of the solution increased by 13.5 °C within 5 min. In contrast, the corresponding cryptocyanine (**CCy**) lacking the triarylphosphonium group gave rise to only an ~3.4 °C increase in solution temperature under otherwise identical conditions. **Mito-CCy** also exhibited high cytotoxicity in HeLa cells when subject to photoirradiation. This light-induced cytotoxicity is attributed to the endogenous production of reactive oxygen species (ROS) induced under conditions of local heating. ROS are known to interfere with the mitochondrial defense system and to trigger apoptosis. By targeting the mitochondria, the present sensitizer-based photothermogenic approach is rendered more effective. As such, the system reported here represents the vanguard of what might be a new generation of organelle-targeted photothermal therapeutics.

Graphical abstract

[*]**Corresponding Authors:** sessler@cm.utexas.edu, kangch@khu.ac.kr, jongskim@korea.ac.kr.

Supporting Information

The Supporting Information is available free of charge on the ACS Publications website at DOI: 10.1021/jacs.7b04263. Detailed experimental conditions and methods, synthesis, structural characterization, spectroscopic analyses, functional characterization of cryptocyanines, and biological evaluations (PDF)

ORCID

Jonathan L. Sessler: 0000-0002-9576-1325

Notes

The authors declare no competing financial interest.

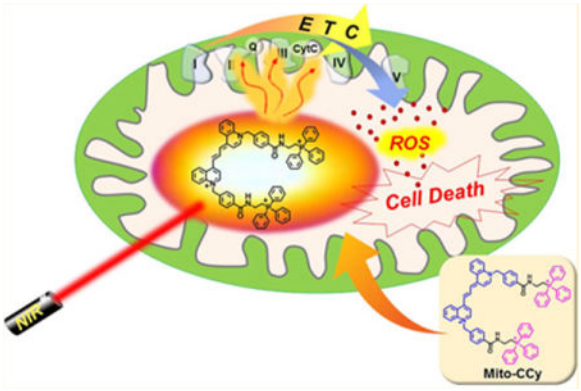

INTRODUCTION

Phototherapy is a light-induced therapeutic modality, which traditionally includes photodynamic therapy (PDT) and photothermal therapy (PTT). In both, chemical agents are used as photosensitizers that then produce either reactive oxygen species (ROS) or induce heat shock, or a combination thereof.[1,2] These methods continue to attract the attention of researchers engaged in cancer therapy, as a number of cancers have been found to be particularly sensitive to these types of treatment.[3,4] To date, more attention has focused on PDT than on PTT; indeed, several PDT photosensitizers have received the US Food and Drug Administration (FDA) approval for specific indications. However, PTT has emerged as a potentially safer option. This is because off-target sensitizing effects and irreversible oxidative damage beyond the targeted cancer locus is often seen in the course of PDT.[1,3,5] Additionally, PDT, as practiced clinically, requires an adequate tumor oxygen supply.[5] This can limit its efficiency in hypoxic environments, whereas PTT does not suffer from this drawback. In many instances, PTT effects can be produced using dyes in the near-infrared (NIR) spectral region, which further lowers damage to tissues surrounding the tumor targets of interest. It is thus suggested that PTT could emerge as a less invasive treatment option than not only PDT, but also current standards of care, such as, e.g., radiation or chemotheraphy.[2,6,7] Not surprisingly, therefore, considerable effort is being devoted to the study of new potential PTT sensitizers.

To date, nanomaterials, including transition metal oxides,[8] sulfide nanoparticles,[9] gold nanoparticles,[10] platinum nanoparticles,[11] and nanocarbon species,[12,13] have been studied as photosensitizers in PTT. Their compatibility with NIR irradiation and excellent photothermal conversion efficiency, combined with high absorption and superior photostability, are appealing features. However, the poor biodegradability and potential long-term toxicity of many nanomaterials represent potential limitations to clinical translation efforts.[14] Organic photosensitizers, such as cyanines,[15,16] formulated in micelles or liposomes[17,18] or conjugated to polymers,[19,20] have thus been studied as potential alternative PTT photosensitizers. Their safety is reflected by the US FDA's decision to approve indocyanine green (ICG) as a medical imaging agent. ICG has since been used off-label as a PTT agent.[18] However, PTT is not devoid of issues. In particular, the relatively high temperatures needed to produce a robust cancer effect via PTT can increase damage to

surrounding normal cells.[21] In addition, many of the existing agents suffer from poor inherent biolocalization features, which can limit their utility. Agents that combine singlet oxygen generation with thermal production could obviate some of these concerns.[22] Also attractive would be PTT agents that localize specifically to particularly susceptible organelles. With these considerations in mind, we have developed a new, mitochondria-targeted PTT sensitizer based on cryptocyanine. This system, referred to as **Mito-CCy**, displays a high photothermal conversion efficiency, good biological compatibility *in vitro*, and photoinduced cytotoxicity in HeLa cells that is ascribed in part to organelle-specific endogenous ROS production.

Mitochondria are indispensable cellular organelles responsible for the production of the majority of the cell's energy supply. They also play a key role in programed cell death such as apoptosis. These organelles are particularly sensitive to changes in cardiolipin metabolism[23] or heat shock[24,25] and are easily damaged by ROS formation.[26,27] Therefore, mitochondrial heat delivery mediated through various forms of nanostructures[28–30] has been attempted by adopting mitochondrial-guiding agents (e.g., triarylphosphonium (TPP) cations,[31] mitochondrial phospholipid cardiolipin,[32] mitochondria-penetrating peptides,[33] an oligomeric carbohydrate scaffold,[34] mitochondrial targeting sequences,[34] and a vesicle-based transporter system[34]). Recently, we reported a mitochondrial targeting hyperthermia-inducing agent using TPP-conjugated nanoparticles that induced mitochondrial dysfunction, resulting in apoptosis.[8] However, small organic molecules offer advantages relative to other nanomaterials, including in many instances improved safety as well as ease of preparation and modification. We therefore suggest that mitochondria-targeting PTT agents based on organic molecules might provide significant benefits. However, to our knowledge, such systems have yet to be reported.

In this study, we set out to explore the potential benefits associated with a small molecule-based approach to mitochondria-localized PTT. Toward this end, the putative mitochondria targeting NIR-thermogenic cryptocyanine dye (**Mito-CCy**) was prepared (cf. Figure 1). **Mito-CCy** was designed to fulfill two critical requirements expected to maximize the PTT efficiency: (i) efficient light absorption but a low fluorescence quantum yield (QY), as well as a low singlet oxygen QY, so as to maximize the conversion of absorbed photoenergy into thermal energy[35] and (ii) mitochondrial localization of the photo-sensitizer to enhance the presumed photocytotoxicity.[8,28–30] As detailed below, the absorption spectrum of **Mito-CCy** is characterized by an intense NIR absorption band and a low fluorescence QY (<0.01), as well as a low singlet oxygen QY (<0.02). It also possesses lipophilic cationic parts to enhance mitochondrial targeting.[36] Despite the low QY of **Mito-CCy**, it still proved possible to visualize its fluorescence *in vitro* by means of confocal microscopy. This allowed the real-time monitoring of its uptake by the mitochondria. Subsequent NIR light irradiation generates heat and, in conjunction with endogenous ROS production, results in mitochondrial dysfunction and cell apoptosis as outlined in Figure 1.

RESULTS AND DISCUSSION

Synthesis and Characterization of Cryptocyanines

The putative mitochondria-targeted cryptocyanine (**Mito-CCy**) and a nontargeted cryptocyanine (**CCy**) control were synthesized as outlined in Figure 2. Briefly, the synthesis entailed the alkylation of 4-methylquinoline with 4-bromomethylbenzoic acid to yield **3**, which was further reacted with *N,N′*-diphenylformamidine and acetic anhydride to produce **2**. Extension of the π-conjugated system **2** with **3** and triethylamine (TEA) resulted in cryptocyanine **1**. The amide-linked target compound, **Mito-CCy**, was obtained from **1** by reacting with $(PPh_3{}^+(CH_2)_2NH_2)Br^-$ in the presence of 2-(1*H*-9-azobenzo-triazole-1-yl)-1,1,3,3-tetramethylammonium hexafluorophosphate (HATU), diisopropylethylamine (DIPEA), and TEA in *N,N*-dimethylformamide (DMF). **CCy**, an analogue lacking the TPP unit, was prepared using an analogous procedure. Both **Mito-CCy** and **CCy** and gave ^{1}H NMR and ^{13}C NMR spectral and ESI-MS analytical data consistent with their proposed structures (Figures S26–S40).

Spectroscopy

The absorption and emission features of **Mito-CCy** and **CCy** were probed in dimethyl sulfoxide (DMSO) using UV–vis and fluorescence spectroscopy, respectively (Figure 3). The absorption spectra exhibited an intense peak at 713 nm with large molar extinction coefficients of 15.5×10^4 M^{-1} cm^{-1} and 17.0×10^4 M^{-1} cm^{-1} for **Mito-CCy** and **CCy**, respectively (Figure S1). In the case of both probes, the fluorescence maximum was observed at 734 nm (Figure 3). The fluorescence QYs (Φ_f) of **Mito-CCy** and **CCy** were calculated according to eq S1 and found to be 0.007 and 0.011, respectively. These values are in agreement with what has been reported for other dyes sharing the same basic cryptocyanine scaffold.[37] As shown in Figure S2, the two cryptocyanines, **Mito-CCy** and **CCy**, also exhibited large molar extinction coefficients in the NIR region in other common solvents such as CH_2Cl_2, CH_3CN, MeOH, and water. The emission maxima of these probes showed slight variations as a function of solvent, with modest bathochromic shifts (<20 nm) being seen upon increasing solvent polarity from CH_2Cl_2 to H_2O.

Whereas the UV–vis absorption features of either **Mito-CCy** or **CCy** were not appreciable affected by the choice of organic solvents, in aqueous media variations were seen in the optical signature of **CCy** as a function of the ionic strength. This latter finding was ascribed to their limited solubility in aqueous environments. As shown in Figure 3d–e, the spectra of both **Mito-CCy** and **CCy** exhibit an intense peak at 702 nm in aqueous media containing 10% DMSO. However, in a solution of higher ionic strength (10 mM PBS various pH conditions) a hypsochromic shift in the absorption maximum (~200 nm) with an associated color change from green to purple (Figure 3f–g and Figure S3) was seen for **CCy**. The absorption bands of **CCy** show similarly hypsochromic shifts in various buffer solutions (e.g., HEPES, MES, monosodium phosphate, and Tris) (Figure S4). Similar spectral behavior was seen for more biomimetic **CCy** solutions, including those containing CT-DNA (50 μg/mL) or HeLa cell cytosol extract (20 μg/mL) (Figure S5). These results led us to suggest that the observed spectral shifts are not caused by the choice of buffering agent. Rather, the hypsochromic shifts in the absorption maxima of **CCy** are ascribed to

aggregation effects that are likely to be relatively enhanced in aqueous environments. Support for this latter conclusion comes from an observation of similar shifts in dye molecules that interact in a face-to-face manner to form so-called H-aggregates.[38–40] However, aggregation is not a desirable feature for PTT agents since it can lead to reduced heat transfer. Fortunately, no evidence of aggregation was seen for **Mito-CCy** (as opposed to **CCy**) under any of these conditions (Figures 3 and S3–S5). This desirable lack of aggregation is rationalized in terms of the presence of the cationic phosphonium substituents, which provide for electrostatic repulsion between the individual monomers.

Photothermal Conversion Efficiency

The fluorescence QYs (Φ_f) of **Mito-CCy** (0.007) and **CCy** (0.011) tabulated in Figure 3a are much lower than that of the FDA-approved agent ICG (0.078) (cf. Table S1).[41] To obtain insights into the relative photothermal capability of the present cryptocyanines as compared to ICG, their conversion efficiencies were compared under conditions of 730 nm laser irradiation, using DMSO as the solvent to ensure complete solubilization of both photosensitizers. The temperature of the **Mito-CCy** (0.5 mM) solution was raised by 24.5 °C upon irradiation for 5 min at 730 nm laser irradiation (3.0 W/cm^2). Moreover, the extent of temperature increase was found to correlate well with the laser power (Figure 4a–b) as well as the **Mito-CCy**'s concentration (Figure 4c–d). Similar photothermal efficiencies were observed for **CCy** (Figure S6).

To evaluate the heat transfer utility of the cryptocyanines, their photothermal conversion efficiencies (η) were measured following a reported method.[42] Briefly, under conditions of 730 nm laser irradiation (2.3 W/cm^2), the temperature of the solution including the cryptocyanines (0.5 mM) was allowed to increase to the point of steady state. After switching the laser off, the temperature decrease was recorded so as to estimate the heat transfer rate from the solution to the environment (Figures 4e–f and S6e–f). As defined by eq S2, the efficiencies (η) of **Mito-CCy** and **CCy** were found to be approximately 9.5% and 8.4%, respectively, and thus approximately 3-fold higher than the value reported for ICG (~3.1%; cf. Table S1). The enhanced photothermal efficiencies seen for **Mito-CCy** and **CCy** relative to ICG are consistent with their lower fluorescence quantum yields, which is expected to allow a greater nonemissive conversion of NIR light into heat.

Photochemical Properties of Mito-CCy and CCy

Prior to applying of the cryptocyanines to *in vitro* based PTT studies, we investigated their basic chemical and photochemical features. First, the ROS generating ability of the cryptocyanines was estimated by quantifying the singlet oxygen coproduction under conditions of photoirradiation. The coproduction of ROS during PTT has been advanced as being both advantageous in terms of increased cytotoxicity at lower temperatures[22] and problematic due triggering undesired side-effects.[43] The singlet oxygen QYs (Φ_Δ) of **Mito-CCy** and **CCy** were determined according to eq S6 and were found to be 0.015 and 0.018, respectively, upon irradiation at 730 nm (Figure S7). These QYs (Φ_Δ) are small compared to those of dyes that are used clinically, such as methylene blue (MB) (0.52 in DMSO, Figure S8).[44] Moreover, the singlet oxygen QY of **Mito-CCy** is ~4.3 times lower than that of ICG (Φ_Δ = 0.065, Figure S9), a potential photosensitizer with a negligible singlet oxygen QY.[45]

Low QYs for **Mito-CCy** and **CCy** were also found in more biomimetic media produced by the addition of calf thymus DNA (50 μg/mL) to PBS or in the HeLa cell cytosol extract (20 μg/mL) (Figures S12–15). Given the low singlet oxygen QYs seen for **Mito-CCy** and **CCy** and the fact that **Mito-CCy** is less effective at producing singlet oxygen than ICG, we rule out the direct production of significant quantities of ROS when our probes are subject to photoactivation.

The photostability of **Mito-CCy** and **CCy** was also investigated. Toward this end, these two cryptocyanines were subject to repeated irradiation–cooling cycles using 730 nm laser irradiation (2.3 W/cm^2) for 1 h followed by passive cooling to room temperature. As shown in Figure 5a–d, the variation in the maximal temperature increase during each cycle proved to be less than 2.0%, leading us to conclude that **Mito-CCy** and **CCy** are stable under conditions of 730 nm laser irradiation.

Consistent with the relatively nonaggregated nature of **Mito-CCy** in aqueous media (cf. Figure 3f–g), a buffer solution of **Mito-CCy** leads to a higher temperature elevation than a corresponding one containing **CCy** when studied under identical conditions (~13.5 °C vs ~3.4 °C for **Mito-CCy** and for **CCy**) (Figure 6a–b). Similar temperature elevation effects were observed for **Mito-CCy** and **CCy** in more biomimetic media containing calf thymus DNA (50 μg/mL) (~11.1 °C vs ~3.1 °C for **Mito-CCy** and for **CCy**) or HeLa cell cytosolic extract (20 μg/mL) (~11.1 °C vs ~2.4 °C for **Mito-CCy** and for **CCy**) over the course of 5 min (Figure S16). On the basis of these findings, we considered it likely that **Mito-CCy** would prove effective as a PTT agent *in vitro*.

Cellular Localization of Mito-CCy

Prior to investigating the presumed photothermal cytotoxicity of **Mito-CCy** *in vitro*, the intracellular location of **Mito-CCy** was determined in HeLa cells using fluorescence confocal microscopy and various commercially available organelle-selective trackers. As can be seen from an inspection of Figure 7, the fluorescence image of **Mito-CCy** overlaps well with that of a commercially available mitochondrial tracking dye, MitoTracker Green FM. However, poorer overlap was seen in the case of ER- or Lyso-Tracker. The corresponding Pearson Correlation (PC) coefficients are 0.95, 0.64, and 0.44 for these three probes, respectively. These results provide support for the notion that **Mito-CCy** localizes in mitochondria, presumably as the result of the cationic appended triarylphosphonium moieties that help direct the dye to the mitochondrion.[36]

We further confirmed mitochondrial localization of **Mito-CCy** at various postincubation times (1, 2, 4, and 20 h). At 1 h postincubation of **Mito-CCy**, the PC value for mitochondrial localization was 0.80, presumably reflecting some residual adherence of the agent at or near the cell plasma membrane (Figure S17). At later times, the fluorescent image overlapped well with that of MitoTracker (PCs: 0.91, 0.95, and 0.92 for 2, 4, and 20 h incubation, respectively) (Figure S17). From these results, we infer no significant relocalization behavior up to 20 h and thus conclude that **Mito-CCy** may be used to achieve mitochondria targeting under our experimental conditions.

Photothermal Cytotoxicity of Mito-CCy in Cells

The cytotoxicity of **Mito-CCy** was tested by incubating HeLa cells with the presumed PTT sensitizer and subjecting to NIR irradiation. Propidium iodide (PI), an indicator of dead cells, was used to judge cell killing efficacy. As can be seen from an inspection of Figure 8a, the number of PI-positive cells observed upon photoirradiation gradually increases as a function of **Mito-CCy** concentration in the cell medium, whereas few PI-positive red signals were seen in the case of the dark studies (Figure S19). A quantitative analysis of the proportion of PI-positive cells is shown in Figure 8b. Here, the dead cells give rise to positive PI staining. The total number of cells was determined by staining with Hoechst 33342, a dye that allows nuclei to be visualized regardless of their viability status (cf. Figure S20). The cytotoxic effect produced by **Mito-CCy** is localized within the photoirradiated region as shown in Figure 8c. In this figure, many red PI-fluorescence spots were found in the photoirradiated region whereas cells not subject to photoirradiation remained viable. We thus conclude that **Mito-CCy** showed no significant cytotoxicity in the dark but gives rise to cytotoxicity upon photoirradiation.

Photoinduced ROS Formation by Mito-CCy and Its Mechanism

To investigate the mechanism of the cytotoxicity by photoirradiation of **Mito-CCy** in Figure 8, the mitochondrial ROS levels were measured using MitoSOX, a mitochondrial ROS sensor. Indeed, the fluorescent intensity of MitoSOX is elevated upon 730 nm NIR irradiation (Figure 9b–c) whereas *N*-acetylcysteine (NAC), a ROS scavenger,[46] dramatically decreased the emission (Figure S21). These results are taken as evidence that ROS plays a role in mediating the cytotoxicity produced by **Mito-CCy** under photothermal activation. On the other hand, considering that **Mito-CCy** is an ineffective ROS photosensitizer (see Figures S7, S10, S12, and S14) but an efficient photothermal agent (see also Figures 6 and S16), we suggest that the cytotoxic ROS production seen in the case of **Mito-CCy** (cf. Figure 9b–c) is not the result of direct ROS produced by photoirradiation; rather, it comes from the generated heat.

One concern associated with relying on thermal effects to produce ROS is that the associated heat might damage enzymes, such as superoxide dismutase (SOD), that provide protection against ROS. To the extent this occurs, it may complicate efforts to ascertain the mechanistic determinants of the putative cytotoxicity. To address this concern, ROS formation was measured using MitoSOX in the presence of a potent SOD inhibitor, 2-methoxyestradiol.[47] The results, shown in Figure S22, reveal that upon irradiation in the absence of **Mito-CCy**, addition of the estradiol inhibitor served to increase slightly the emission intensity of MitoSOX relative to the control. However, the addition of the inhibitor enhanced dramatically the ROS induced by **Mito-CCy** under identical conditions of irradiation. We interpret these results in terms of the estradiol SOD inhibitor contributing to mitochondrial ROS generation in a manner that is independent from the action of **Mito-CCy**. We thus consider it unlikely that **Mito-CCy** mediates its action by deactivating SOD or other protective enzymes present in the mitochondria.

We next sought to determine whether **Mito-CCy**-mediated PTT perturbs the respiratory electron transfer chain. Toward this end, the ROS levels were measured when **Mito-CCy**

was photoirradiated in the absence and presence of rotenone, antimycin A, or both. These agents are potent inhibitors of the mitochondrial respiratory chain complexes I and III,[48] respectively. As shown in Figure 9c(iv), in the presence of both inhibitors, the ROS levels in the cells decreased dramatically under conditions of photoirradiation. In light of this result, we conclude that PTT-mediated ROS generation in mitochondria requires an electron transport chain that functions in whole or in part and that the photoaction of **Mito-CCy** originates from its photothermal effect.

We also found that the fluorescence intensity of **Mito-CCy** was not altered after being incubated for 30 min in the presence of rotenone and antimycin A (Figure S24) and that the fluorescence signal ascribed to **Mito-CCy** was still localized in the mitochondria after treatment with both inhibitors (Figure S25), as well as in their absence. We thus conclude that **Mito-CCy** is subject to negligible efflux under the conditions of these experiments, in spite of the reduced membrane potential caused by the inhibitors. This, in turn, leads us to rule out the possibility that the variations in the ROS levels induced by the inhibitors rotenone and antimycin A are caused by reductions in effective photosensitizer concentration.

Many other photochemical therapeutic agents are reported to involve ROS generation that could also originate in the mitochondrion.[8,30] As such, the results in this study lead us to suggest that it may be necessary to reconsider whether the ROS generating capabilities of other photosensitizers are direct (i.e., originate from their photoactivation and ROS production) or are indirect and involve perturbations of mitochondrial respiration events stimulated through a photothermal effect.

CONCLUSIONS

To the best of our knowledge, this work is the first report wherein the mitochondria is targeted as the primary site of action for a NIR irradiation-activated cryptocyanine dye. The new PTT agent reported here, **Mito-CCy**, contains two functional components, namely a triarylphosphonium mitochondrial localizing unit and a cryptocyanine photosensitizer. Based on fluorescence microscopy, it was determined that **Mito-CCy** localizes preferentially in the mitochondria of HeLa cells. When subject to 730 nm photoirradiation, **Mito-CCy** produces an increase in temperature in test systems. This increase is dependent on both the laser power and probe concentration. It is much more effective in terms of photothermal conversion than a congeneric control system, **CCy**, that, in contrast to **Mito-CCy**, is aggregated in aqueous media. When HeLa cells are incubated with **Mito-CCy** and subject to photoirradiation, cytotoxicity is observed. On the basis of ROS detection experiments and control studies involving inhibition of the mitochondrial respiratory chain, it is concluded that the **Mito-CCy**-induced PTT cytotoxicity is due to endogenous ROS generation, rather than direct ROS production. The present study thus leads us to suggest that systems such as **Mito-CCy**, which take advantage of thermally induced mitochondrial-based ROS production to mediate cell killing, could represent promising PTT photosensitizers. We believe this work provides an important starting point for creating cryptocyanine-based PTT agents. More broadly, we believe the present studies provide important mechanistic insights

that could help drive further advances in the area of sensitizer-based anticancer research and treatments.

Supplementary Material

Refer to Web version on PubMed Central for supplementary material.

Acknowledgments

This work was supported by CRI project (No. 2009-0081566, J.S.K.) and the Basic Science Research Programs (2015R1A6A3A04058789, H.S.J. and 2014R1A21A11052325, C.K.) from the National Research Foundation of Korea (NRF) funded by the Ministry of Education. The work in Austin was supported by the National Institutes of Health (CA68682, J.L.S.) and the Robert A. Welch Foundation.

References

1. Dolmans DE, Fukumura D, Jain RK. Nat Rev Cancer. 2003; 3:380–387. [PubMed: 12724736]
2. Lal S, Clare SE, Halas NJ. Acc Chem Res. 2008; 41:1842–1851. [PubMed: 19053240]
3. Trachootham D, Alexandre J, Huang P. Nat Rev Drug Discovery. 2009; 8:579–591. [PubMed: 19478820]
4. Robins, HI. New Directions in Cancer Treatment. Magrath, I., editor. Springer Berlin Heidelberg; Berlin, Heidelberg, Germany: 1989. p. 85-92.
5. Casas, A., Perotti, C., Di Venosa, G., Batlle, A. Resistance to Photodynamic Therapy in Cancer. Rapozzi, V., Jori, G., editors. Springer International Publishing; Cham, Switzerland: 2015. p. 29-63.
6. O'Neal DP, Hirsch LR, Halas NJ, Payne JD, West JL. Cancer Lett. 2004; 209:171–176. [PubMed: 15159019]
7. Melancon MP, Zhou M, Li C. Acc Chem Res. 2011; 44:947–956. [PubMed: 21848277]
8. Jung HS, Han J, Lee J-H, Lee JH, Choi J-M, Kweon H-S, Han JH, Kim J-H, Byun KM, Jung JH, Kang C, Kim JS. J Am Chem Soc. 2015; 137:3017–3023. [PubMed: 25662739]
9. Zhou M, Zhang R, Huang M, Lu W, Song S, Melancon MP, Tian M, Liang D, Li C. J Am Chem Soc. 2010; 132:15351–15358. [PubMed: 20942456]
10. Wang S, Huang P, Nie L, Xing R, Liu D, Wang Z, Lin J, Chen S, Niu G, Lu G, Chen X. Adv Mater. 2013; 25:3055–3061. [PubMed: 23404693]
11. Porcel E, Liehn S, Remita H, Usami N, Kobayashi K, Furusawa Y, Le Sech C, Lacombe S. Nanotechnology. 2010; 21:85103. [PubMed: 20101074]
12. Yang K, Zhang S, Zhang G, Sun X, Lee ST, Liu Z. Nano Lett. 2010; 10:3318–3323. [PubMed: 20684528]
13. Robinson JT, Welsher K, Tabakman SM, Sherlock SP, Wang H, Luong R, Dai H. Nano Res. 2010; 3:779–793. [PubMed: 21804931]
14. Song X, Chen Q, Liu Z. Nano Res. 2015; 8:340–354.
15. Shi C, Wu JB, Pan D. J Biomed Opt. 2016; 21:050901.
16. Wu JB, Lin TP, Gallagher JD, Kushal S, Chung LW, Zhau HE, Olenyuk BZ, Shih JC. J Am Chem Soc. 2015; 137:2366–2374. [PubMed: 25585152]
17. Yu J, Javier D, Yaseen MA, Nitin N, Richards-Kortum R, Anvari B, Wong MS. J Am Chem Soc. 2010; 132:1929–1938. [PubMed: 20092330]
18. Sheng, Z., Zheng, M., Cai, L. Biomedical Nanomaterials. Zhao, Y., Shen, Y., editors. Wiley-VCH Verlag GmbH & Co. KGaA; Weinheim, Germany: 2016. p. 177-206.
19. Yang K, Xu H, Cheng L, Sun CY, Wang J, Liu Z. Adv Mater. 2012; 24:5586–5592. [PubMed: 22907876]
20. Cheng L, Yang K, Chen Q, Liu Z. ACS Nano. 2012; 6:5605–5613. [PubMed: 22616847]
21. Fajardo LF. Cancer Res. 1984; 44:4826s–4835s. [PubMed: 6467235]

22. Yoo D, Jeong H, Preihs C, Choi JS, Shin TH, Sessler JL, Cheon J. Angew Chem, Int Ed. 2012; 51:12482–12485.
23. Wright MM, Howe AG, Zaremberg V. Biochem Cell Biol. 2004; 82:18–26. [PubMed: 15052325]
24. Flanagan SW, Moseley PL, Buettner GR. FEBS Lett. 1998; 431:285–286. [PubMed: 9708920]
25. Wang Z, Cai F, Chen X, Luo M, Hu L, Lu Y. PLoS One. 2013; 8:e75044. [PubMed: 24023970]
26. Murphy MP. Biochem J. 2009; 417:1–13. [PubMed: 19061483]
27. Murphy MP. Biochem Soc Trans. 2016; 44:1219–1226. [PubMed: 27911703]
28. Zhou F, Wu S, Wu B, Chen WR, Xing D. Small. 2011; 7:2727–2735. [PubMed: 21861293]
29. Chen S, Lei Q, Qiu W-X, Liu L-H, Zheng D-W, Fan J-X, Rong L, Sun Y-X, Zhang X-Z. Biomaterials. 2017; 117:92–104. [PubMed: 27939904]
30. Shah BP, Pasquale N, De GJ, Tan T, Ma JJ, Lee KB. ACS Nano. 2014; 8:9379–9387. [PubMed: 25133971]
31. Murphy MP, Smith RAJ. Annu Rev Pharmacol Toxicol. 2007; 47:629–656. [PubMed: 17014364]
32. Hoye AT, Davoren JE, Wipf P, Fink MP, Kagan VE. Acc Chem Res. 2008; 41:87–97. [PubMed: 18193822]
33. Horton KL, Stewart KM, Fonseca SB, Guo Q, Kelley SO. Chem Biol. 2008; 15:375–382. [PubMed: 18420144]
34. Yousif LF, Stewart KM, Kelley SO. ChemBioChem. 2009; 10:1939–1950. [PubMed: 19637148]
35. Shao, A., Wu, X., Zhu, W. Near-infrared Nanomaterials: Preparation, Bioimaging and Therapy Applications. Zhang, F., editor. RSC Publishing; Cambridge, United Kingdom: 2016. p. 125-157.
36. Smith RAJ, Hartley RC, Murphy MP. Antioxid Redox Signaling. 2011; 15:3021–3038.
37. Rurack K, Spieles M. Anal Chem. 2011; 83:1232–1242. [PubMed: 21250654]
38. Czikklely V, Forsterling HD, Kuhn H. Chem Phys Lett. 1970; 6:207–210.
39. Nüesch F, Grätzel M. Chem Phys. 1995; 193:1–2.
40. Kumar V, Baker GA, Pandey S. Chem Commun. 2011; 47:4730–4732.
41. Philip R, Penzkofer A, Baumler W, Szeimies RM, Abels C. J Photochem Photobiol, A. 1996; 96:137–148.
42. Tian QW, Jiang FR, Zou RJ, Liu Q, Chen ZG, Zhu MF, Yang SP, Wang JL, Wang JH, Hu JQ. ACS Nano. 2011; 5:9761–9771. [PubMed: 22059851]
43. Guha S, Shaw SK, Spence GT, Roland FM, Smith BD. Langmuir. 2015; 31:7826–7834. [PubMed: 26149326]
44. Hu Q-J, Lu Y-C, Yang C-X, Yan X-P. Chem Commun. 2016; 52:5470–5473.
45. Atchison J, Kamila S, Nesbitt H, Logan KA, Nicholas DM, Fowley C, Davis J, Callan B, McHale AP, Callan JF. Chem Commun. 2017; 53:2009–2012.
46. Halasi M, Wang M, Chavan TS, Gaponenko V, Hay N, Gartel AL. Biochem J. 2013; 454:201–208. [PubMed: 23772801]
47. Huang P, Feng L, Oldham EA, Keating MJ, Plunkett W. Nature. 2000; 407:390–395. [PubMed: 11014196]
48. Chen Q, Vazquez EJ, Moghaddas S, Hoppel CL, Lesnefsky EJ. J Biol Chem. 2003; 278:36027–36031. [PubMed: 12840017]

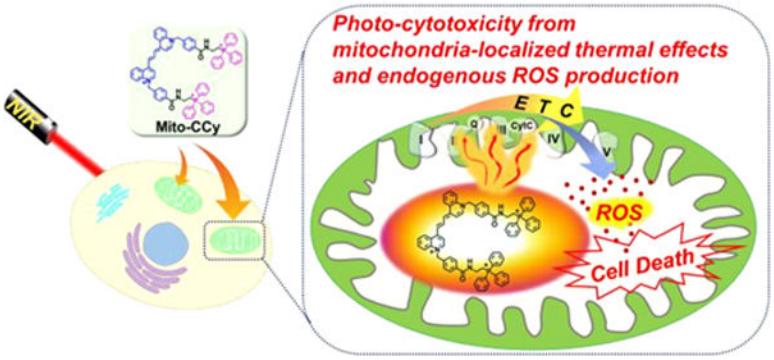

Figure 1.

Schematic representation of enhanced photothermogenesis by mitochondria-targeting cryptocyanine (**Mito-CCy**).

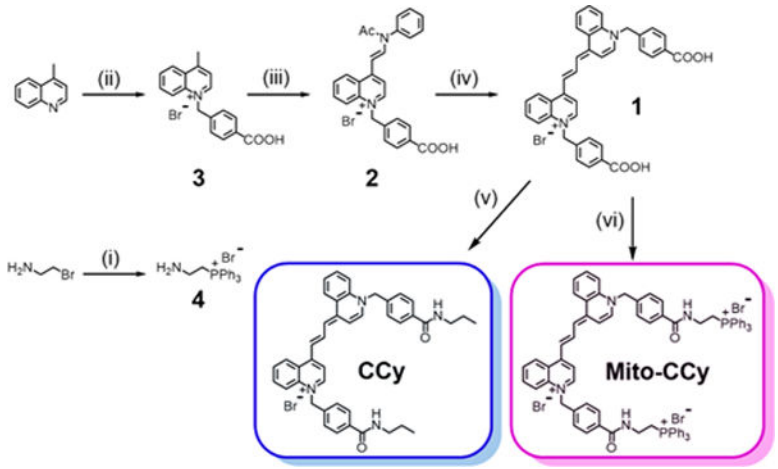

Figure 2.

Synthesis of **Mito-CCy** and **CCy**. (i) Triphenylphosphine, acetonitrile, reflux, 24 h, 88%; (ii) 4-(bromomethyl)benzoic acid, acetonitrile, 110 °C, 6 h, 72%; (iii) *N*,*N*′-diphenylformamidine, acetic anhydride, 150 °C, 1 h, 87%; (iv) **3**, TEA, dichloromethane, 25 °C, 24 h, 46%; (v) propylamine, HATU, TEA, DIPEA, DMF, rt, 24 h, 32%; (vi) **4**, HATU, TEA, DIPEA, DMF, rt, 24 h, 34%.

a

Compound	λ_{abs} (nm)	ε ($\times 10^4$ M^{-1} cm^{-1})	λ_{em} (nm)	Φ_f
Mito-CCy	713	15.5	734	0.007
CCy	713	17.0	734	0.011

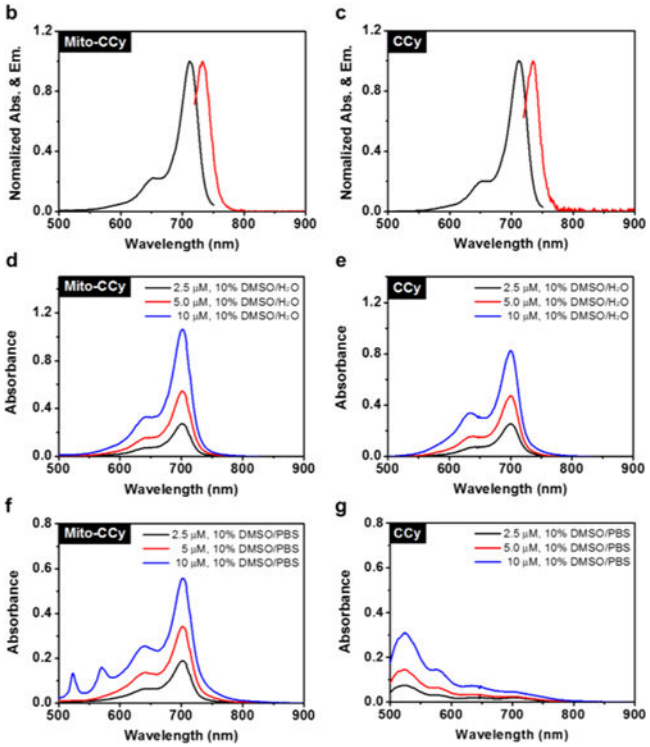

Figure 3.

UV–vis–NIR absorption and emission spectral features of **Mito-CCy** and **CCy**. (a) Photophysical data for **Mito-CCy** and **CCy**. All values were determined in DMSO. ε: molar extinction coefficient ($\times 10^4$ M^{-1} cm^{-1}). λ_{abs}: absorption maximum wavelength (nm). λ_{em}: emission maximum wavelength (nm). Φ_f: fluorescence quantum yield. Normalized absorption (black) and emission spectra (red) of (b) **Mito-CCy** and (c) **CCy**. Absorption spectra of various concentrations (i.e., 2.5, 5.0, and 10 μM) of (d) **Mito-CCy** and (e) **CCy** in 10% DMSO-water solution and (f) **Mito-CCy** and (g) **CCy** in 10% DMSO-buffer solution (pH 7.4, 10 mM PBS).

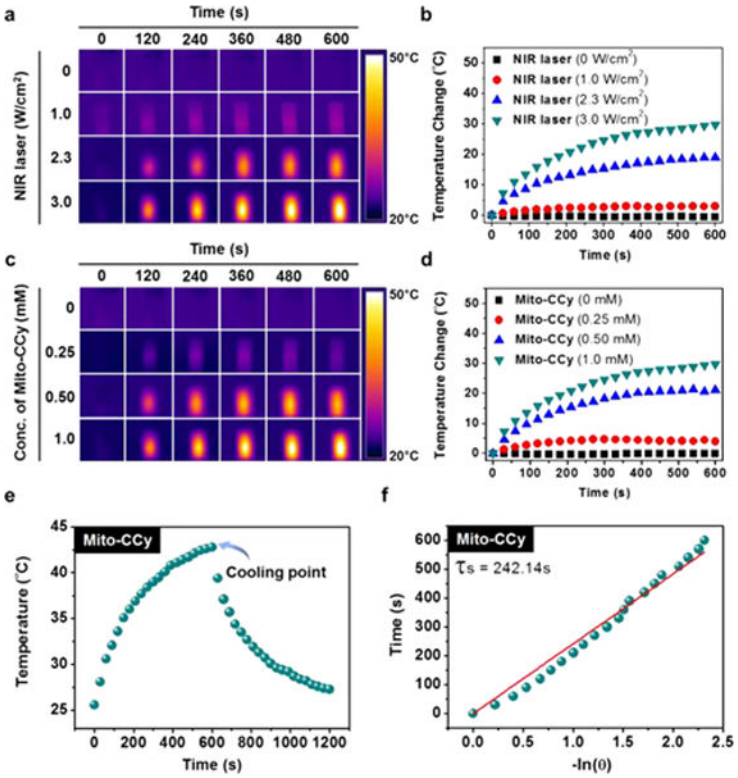

Figure 4.

Photothermal conversion utility of **Mito-CCy**. IR thermal images of DMSO solutions of **Mito-CCy** (a and c). **Mito-CCy** concentration = 0.5 mM and irradiation intensities of 0, 1.0, 2.3, and 3.0 W/cm^2 at 730 nm (a) and 2.3 W/cm^2 irradiation (730 nm) at various **Mito-CCy** concentrations (0, 0.25, 0.50, and 1.0 mM) (c) as a function of irradiation time. Photothermal heating curves for DMSO solutions of **Mito-CCy** at constant 0.5 mM concentrations of **Mito-CCy** and various laser irradiation intensities (0, 1.0, 2.3, and 3.0 W/cm^2, 730 nm) (b) and constant irradiation at 2.3 W/cm^2 with varying **Mito-CCy** concentrations (0, 0.25, 0.50, and 1.0 mM, 730 nm) (d) as a function of irradiation time. Photothermal effects observed upon irradiating **Mito-CCy** with 730 nm laser light (2.3 W/cm^2) for 600 s and then stopping the irradiation (e). Time versus–ln(θ) plot (with θ being the driving force temperature, cf. eq S5) (f) obtained using the data recorded during the cooling period of the experiment outlined in (e). A Ti:Sa femtosecond-pulsed laser (Chameleon XR by Coherent, 200 fs pulse width, 90 MHz repetition rate) was used.

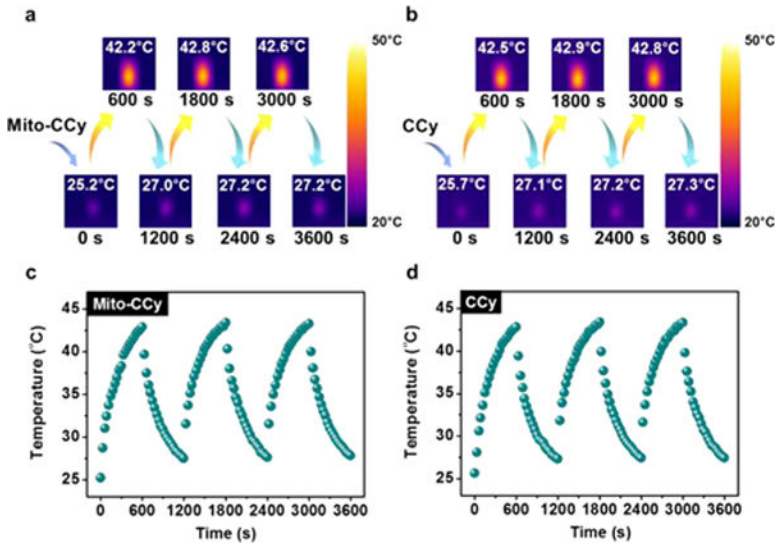

Figure 5.

Photostability of **Mito-CCy** and **CCy** in DMSO. IR thermal images of (a) **Mito-CCy** and (b) **CCy**. Curves showing the temperature change of (c) **Mito-CCy** and (d) **CCy** over several ON/OFF cycles involving irradiation with a 730 nm laser (2.3 W/cm^2) for 1 h followed by passive cooling. A Ti:Sa femtosecond-pulsed laser (Chameleon XR by Coherent, 200 fs pulse width, 90 MHz repetition rate) was used.

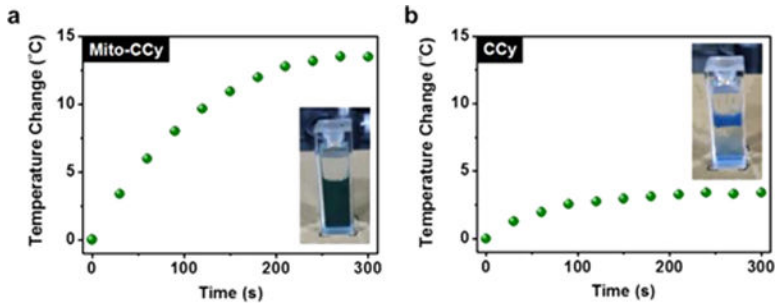

Figure 6.

Photothermal heating curves of **Mito-CCy** and **CCy**. **Mito-CCy** (a) and **CCy** (b) (0.5 mM, respectively) dispersed in 50% DMSO–buffer solution (pH 7.4, 10 mM PBS) with 730 nm laser irradiation (2.3 W/cm^2) as a function of irradiation time. A Ti:Sa femtosecond-pulsed laser (Chameleon XR by Coherent, 200 fs pulse width, 90 MHz repetition rate) was used.

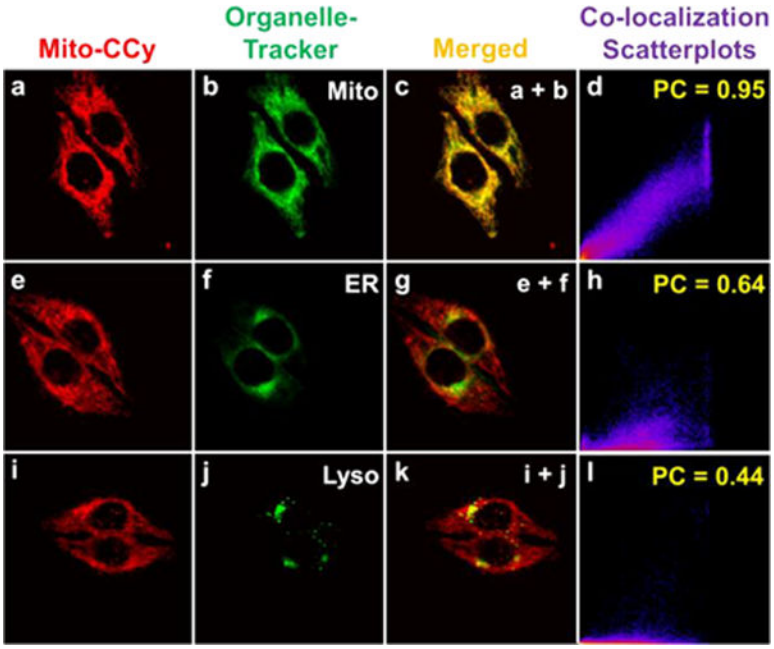

Figure 7.

Confocal microscopic images of **Mito-CCy** colocalized with various commercially available organelle trackers in HeLa cells (a, e, and i). HeLa cells were incubated with **Mito-CCy** (2.0 μM) for 4 h and then with (b) MitoTracker Green FM (0.05 μM), (f) ER Tracker Green (1.0 μM), or (j) Lysotracker Green DND-26 (0.05 μM) for 15 min. (c) Merged image of (a) and (b). (g) Merged image of (e) and (f). (k) Merged image of (i) and (j). (d) Colocalization scatterplots of (c). PC: 0.95. (h) Co-localization scatterplots of (g). PC: 0.64. (l) Co-localization scatterplots of (k). PC: 0.44. The fluorescence images of the organelle trackers and **Mito-CCy** were collected with 488 and 633 nm light being used as the excitation and detection wavelengths, respectively, with 505–530 nm band-pass (green) and 650 nm long pass (red) filters being employed as warranted.

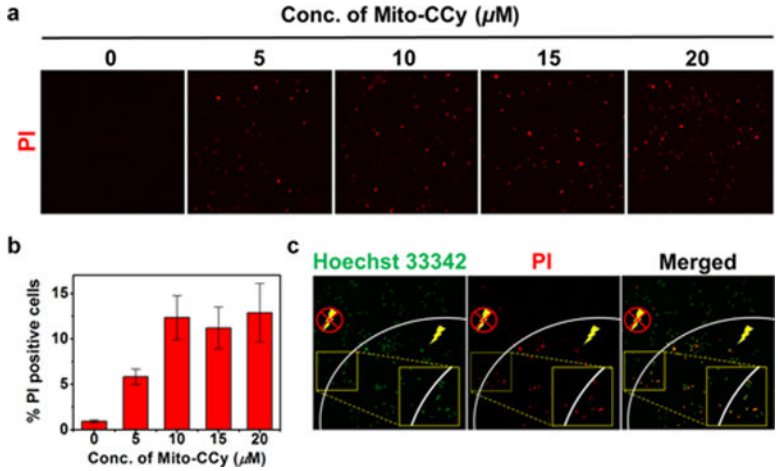

Figure 8.

Effect of NIR irradiation following **Mito-CCy** administration on the viability of HeLa cells. (a) Confocal fluorescence images of propidium iodide-treated HeLa cells after incubation with various concentration of **Mito-CCy** for 4 h, following by 730 nm irradiation (2.3 W/cm^2) for 10 min. (b) The proportion of PI-positive cells was determined from the ratio of PI-positive cells to the total number of cells as determined by Hoechst 33342 staining. (c) Confocal fluorescence images of HeLa cells obtained after incubation with **Mito-CCy** (20 μM) for 4 h following 730 nm laser irradiation (2.3 W/cm^2) for 10 min. Dead cells are labeled in red by PI staining, whereas all cells were visualized using Hoechst 33342 (green). A Ti:Sa femtosecond-pulsed laser (Chameleon XR by Coherent, 200 fs pulse width, 90 MHz repetition rate) was used. The energy density (fluence) was 1380 J/cm^2.

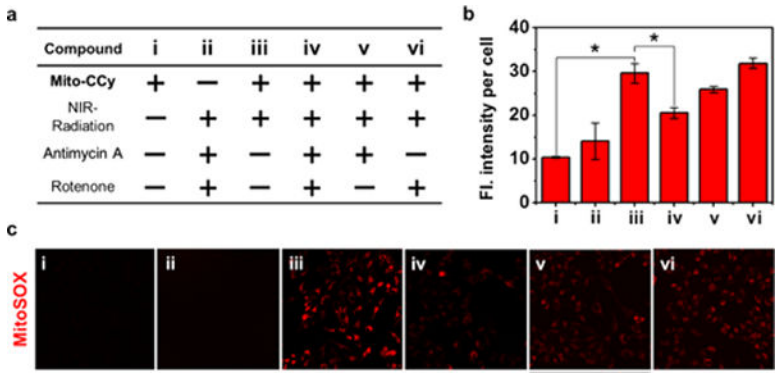

Figure 9.

Use of a ROS indicator to evaluate the production of ROS in mitochondria after incubation of HeLa cells with MitoSOX. (a) Matrix showing experimental design. (b) Fluorescence intensity per cell. $*P < 0.05$. (c) Confocal fluorescence microscopic images of HeLa cells treated with MitoSOX (1.0 μM) according to the treatment variables, including with or without coincubation with **Mito-CCy** (10 μM), 730 nm NIR irradiation (2.3 W/cm^2) for 10 min, antimycin A (0.5 μM), and rotenone (0.5 μM). Fluorescence images were recorded using 488 nm excitation and 550–650 nm emission (red) wavelengths, respectively. A Ti:Sa femtosecond-pulsed laser (Chameleon XR by Coherent, 200 fs pulse width, 90 MHz repetition rate) was used. The energy density (fluence) was 1380 J/cm^2.